Check for updates

JGR Atmospheres

RESEARCH ARTICLE
10.1029/2025JD044828

Effects of Sea Surface Temperature on Tropical Shallow Circulation Strength

Brittany D. Dygert[1] and **Dennis L. Hartmann**[1]

[1]Department of Atmospheric and Climate Science, University of Washington, Seattle, WA, USA

Key Points:

- Both warming the average sea surface temperature and increasing its gradient increase the strength of the shallow circulation
- Warming the sea surface temperature strengthens shallow circulations by enhancing shallow convection
- Increasing the sea surface temperature gradient strengthens shallow circulations by enhancing longwave cooling

Supporting Information:

Supporting Information may be found in the online version of this article.

Correspondence to:

B. D. Dygert,
bdygert@uw.edu

Citation:

Dygert, B. D., & Hartmann, D. L. (2026). Effects of sea surface temperature on tropical shallow circulation strength. *Journal of Geophysical Research: Atmospheres*, *131*, e2025JD044828. https://doi.org/10.1029/2025JD044828

Received 21 JUL 2025
Accepted 23 SEP 2026

Abstract Shallow circulations in the tropics are related to the sea surface temperature distribution, longwave cooling above the boundary layer, and shallow convection in both observations and models. To understand the influences sea surface temperature has on the shallow circulation strength, fixed sea surface temperature distributions are applied in experiments using an idealized general circulation model with uniform insolation and no rotation. The experiments are designed to distinguish the effects of mean sea surface temperature from those of sea surface temperature gradients, creating combinations using global mean SSTs from 299 to 305 K and SST ranges from 2.5 to 15 K. In these simulations, a large-scale, deep circulation develops connecting the coldest to hottest SSTs. Experiments with sufficiently large sea surface temperature mean or range also exhibit a distinct shallow cell above the boundary layer. This shallow cell is associated with a deep moist layer sloping upwards from the coldest to hottest sea surface temperatures. We find that warming the mean sea surface temperature increases the strength and depth of these shallow circulations primarily by increasing shallow convection over intermediate sea surface temperatures, while increasing the sea surface temperature gradient enhances shallow circulation strength primarily by enhancing longwave cooling above the boundary layer.

Plain Language Summary In the tropics, rising motions are driven by latent heat release associated with rainfall over warmer parts of the ocean. These regions of rising motion are connected to regions of sinking motion where the atmosphere is cooled by radiative emission. Atmospheric winds connect the regions of rising and sinking motion, and these circulations play an important role in weather and climate. Some of these circulations are deep and extend from the surface to just below the tropopause, and some are shallow, such that the rising and sinking motion and associated winds are limited to the lower part of the atmosphere. We perform simulations with a global model to explore the effect of mean sea surface temperature (SST) and horizontal gradients of SST on the relative strength of the shallow and deep circulations. We find that the strength and depth of the shallow circulation increases both with the mean SST and the horizontal gradient of SST, but for different reasons. The gradient of SST more strongly affects the radiative cooling in the region of sinking motion, while the mean SST increases the strength of the shallow latent heating in the region of rising motion.

1. Introduction

Understanding the atmospheric circulation in the tropics and its interaction with convection and radiation is critical to the global radiation budget and climate sensitivity (Armour et al., 2024; Bony et al., 2015; Dong et al., 2019). While the predominant view of the tropical circulation envisions a single deep cell, shallow circulations are known to occur in the tropics in both observations and reanalysis data sets (Schulz & Stevens, 2018); the shallow meridional circulation (SMC) on the flanks of the intertropical convergence zone (ITCZ) in the East Pacific is particularly prominent (Huaman et al., 2022; Zhang et al., 2004, 2008). These shallow circulations are characterized by strong return flow above the boundary layer and are often identified in regions with strong sea surface temperature gradients (Zhang et al., 2004). Fläschner et al. (2018) have shown that shallow circulations can have a strong effect on the distribution of precipitation and its response to warming in climate models.

Several studies have investigated the mechanisms underlying these shallow circulations. One potential driver of this shallow circulation is boundary layer pressure gradients created by SST gradients, as in a sea-breeze (Lindzen & Nigam, 1987; Nolan et al., 2007). Other studies find boundary layer radiative cooling to be the best indicator of shallow circulation strength (Naumann et al., 2017; Nishant et al., 2016). Naumann et al. (2017) specifically address the direct impact of sea surface temperature gradients and longwave cooling, and find that longwave cooling is the primary driver. While they found that SST gradients were not strong enough to explain the shallow

© 2026 The Author(s). Journal of Geophysical Research: Atmospheres published by Wiley Periodicals LLC on behalf of American Geophysical Union. This is an open access article under the terms of the Creative Commons Attribution License, which permits use, distribution and reproduction in any medium, provided the original work is properly cited.

21698996, 2026, 20, Downloaded from https://agupubs.onlinelibrary.wiley.com/doi/10.1029/2025JD044828, Wiley Online Library on [23/10/2026]. See the Terms and Conditions (https://onlinelibrary.wiley.com/terms-and-conditions) on Wiley Online Library for rules of use; OA articles are governed by the applicable Creative Commons License

circulation strength through their direct impact on boundary layer pressure gradients, they acknowledge that the longwave cooling increases in experiments with stronger SST gradients due to the effect of SST gradients on the relative humidity distribution. Moving to a smaller scale, Janssens et al. (2024) find that, at the mesoscale, shallow convection is the primary driver of tropical shallow circulations. In their study the SST gradients are relatively weak, and they do not speculate on the potential effects of SST on shallow convection. Discrepancies between these studies are likely partially a product of scale, with SST gradient driven flows representing the largest scale. Convection and circulation are also closely tied in the tropics at larger scales, through a combination of surface moisture convergence and convective instability (Back & Bretherton, 2009; Tomassini, 2020).

Several prior studies using a simplified mock-Walker simulation setup designed to emulate the overturning circulation along the equator have found that a double-cell structure, in which both shallow and deep circulations are present, develops in these simulations (Grabowski et al., 2000; Larson & Hartmann, 2003; Lutsko & Cronin, 2018; Yano et al., 2002). These studies focus on explaining the development of the shallow circulation as primarily being driven by radiative cooling in the subsiding region or shallow convective heating in the rising portion of the shallow cell. Diagnostically, it is difficult to say which of these factors is the primary control on the development of shallow circulations, as both are required to sustain a shallow circulation cell energetically. This problem has recently been addressed in the context of mock-Walker circulations in a convection permitting model by Lutsko and Cronin (2024). They find that a double-cell circulation always develops in this model when surface temperatures are higher than about 300 K, and that the development of the double-cell structure is encouraged by SST gradients. Adding moisture to the subsiding region or fixing the radiative cooling reduces the radiative cooling mechanism and moves the development of the double-cell structure to a higher mean temperature closer to 305 K. This suggests that a mechanism other than radiative cooling also encourages a double-cell structure with a strong shallow circulation when the surface temperature is warm.

Many previous studies have investigated the relationship between SST gradients and circulation. These studies vary from more general interactions between sea surface temperature and circulation strength, to specific effects on the top and bottom heaviness of the distribution (Lindzen & Nigam, 1987; Sobel & Neelin, 2006). Back and Bretherton (2009) use a linear mixed layer model to find that sea surface temperature gradients lead to shallow convergence and convection.

Our goal here is to better understand the comparative roles of mean SST and SST gradients in generating shallow circulations in a tropical context. To do this we use a simplified framework of a global climate model with uniform insolation and no rotation, emulating a global tropical world. We use fixed SST simulations and vary the mean SST and the SST gradient in the domain and compare the shallow versus deep circulations in a suite of experiments in which the mean SST and SST gradient are varied independently. We diagnose the relative roles of radiative cooling and convective heating in driving shallow circulations. We find that SST gradients are important in driving shallow circulations and that the primary energetic support for these shallow circulations is radiative cooling. As the mean SST is increased, however, we see an increasing role for shallow convection in driving shallow circulations. We diagnose the reasons for the increased shallow convection with a convective plume model.

The model and experimental design are described in Section 2. The circulation response to mean SST and SST gradient are described in Section 3.1. The relative humidity distribution and its significance in these experiments is discussed in Section 3.2. The effects of longwave cooling on the circulations are described in Section 4. Diagnosis and interpretation of the effect of shallow convection on shallow circulation strength are given in Section 5. A summary is provided in Section 6.

2. Model and Experiments

These experiments use Geophysical Fluid Dynamics Laboratory's (GFDL) AM2.1 (Anderson et al., 2004). We use a grid with 2 by 2.5° horizontal resolution and 32 vertical levels. We simplify the model by using uniform insolation, no rotation, and prescribed SST. The experiments are spun up until equilibrium, and extended for two decades after equilibrium.

The intention of these experiments is to evaluate the effect of changes in both mean SST and SST range. We prescribe SST with a spatial distribution of wavenumber 1 and mean of 299, 302, 303.5, and 305 K. Experiments using these mean SSTs are run with SST ranges of 2.5, 5, 7.5, 10 and 15 K. Each case is named by its global mean

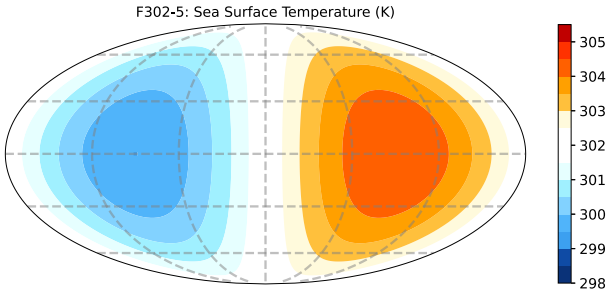


Figure 1. Example of prescribed sea surface temperature (K) in latitude and longitude for F302-5, or the case with a global mean SST of 302 K and a range of 5 K.

SST and SST range. For example, the SST for the case F302-5, is shown in Figure 1, has a global mean SST of 302 K and a SST range of 5 K. The case most closely resembling the current tropics is case F302-5, although the prescribed symmetrical SST distribution we use here is a simplification of the typical left-skewed SST distribution (Hartmann & Dygert, 2022). Cases with higher SST range and mean are more extreme than would be expected from the current tropics.

Moist convection, and particularly the height of convection, is central to these experiments. In AM2.1, this is parameterized using the Relaxed Arakawa-Schubert (RAS) scheme, with the addition of the Tokioka parameter to constrain the activation of deep convection in updrafts without a sufficiently large lateral entrainment rate (Moorthi & Suarez, 1992; Tokioka et al., 1988). AM2.1 treats convection as detraining plumes, where updraft level of detainment determines whether the convection is classified as shallow, deep, or in between. Shallow convection detrains below 800 hPa and deep convection detrains above 500 hPa. Parameter values are linearly interpolated for detrainment levels in between. When we refer to shallow convection in this paper, we are also including midlevel convection that falls into the intermediate range of parameterizations.

The radiative and convective heating of the upper atmosphere over the warmest SSTs are influenced by ice clouds, and thus are sensitive to the microphysical and large-scale parameterization of clouds and precipitation used in the model (Anderson et al., 2004). The cloud microphysics is parameterized by Rotstayn (1997) and Rotstayn et al. (2000) (mixed phase cloud adjustment); large-scale cloud properties by Tiedtke (1993); and the large-scale precipitation by Jakob and Klein (2000).

These experiments have no rotation, and the addition of rotation to tropical RCE experiments introduces cyclones (Carstens & Wing, 2020). Introducing rotation would likely weaken the relationship between the SST gradient and the circulation.

3. Circulation

3.1. Streamfunction

The circulation can be visualized through a mass streamfunction calculated for each case, as shown in Figure 2. Here, we organize the circulation in column relative humidity (CRH) area space, such that the stream function flows from dry to moist regions. The CRH area fraction is then given by

$$\Phi_A(\mathrm{CRH}) = \int_0^{\mathrm{CRH}} f_A d\mathrm{CRH} \tag{1}$$

where f_A is the fraction of the total area of the globe that falls within the CRH bin. The streamfunction is then given by

$$\Psi(\Phi_A, p) = \frac{A_E}{g} \int_0^{\Phi_A} \omega(p) d\Phi'_A \tag{2}$$

where A_E is the global area, g is the gravitational constant, and ω is the vertical velocity in Pa/s at a specific pressure level, p.

This is the same expression used in Hartmann and Dygert (2022) with CRH area fraction in place of SST area fraction. CRH was chosen here because in the cases with small SST gradients the circulation is not well organized by SST, and CRH better captures the contrast between regions of rising and sinking motion. In those cases with larger SST contrast, using CRH area fraction or SST area fraction yield similar results.

In Figure 2 the mean SST increases from left to right and the SST contrast increases from bottom to top. Cases with sufficiently large mean SST or SST range begin to show a double cell structure in which there is a shallow cell distinct from the upper cell. In all cases with sufficiently large SST mean or range, as the global mean SST

21698996, 2026, 20, Downloaded from https://agupubs.onlinelibrary.wiley.com/doi/10.1029/2025JD044828, Wiley Online Library on [23/10/2026]. See the Terms and Conditions (https://onlinelibrary.wiley.com/terms-and-conditions) on Wiley Online Library for rules of use; OA articles are governed by the applicable Creative Commons License

21698996, 2026, 20, Downloaded from https://agupubs.onlinelibrary.wiley.com/doi/10.1029/2025JD044828, Wiley Online Library on [23/10/2026]. See the Terms and Conditions (https://onlinelibrary.wiley.com/terms-and-conditions) on Wiley Online Library for rules of use; OA articles are governed by the applicable Creative Commons License

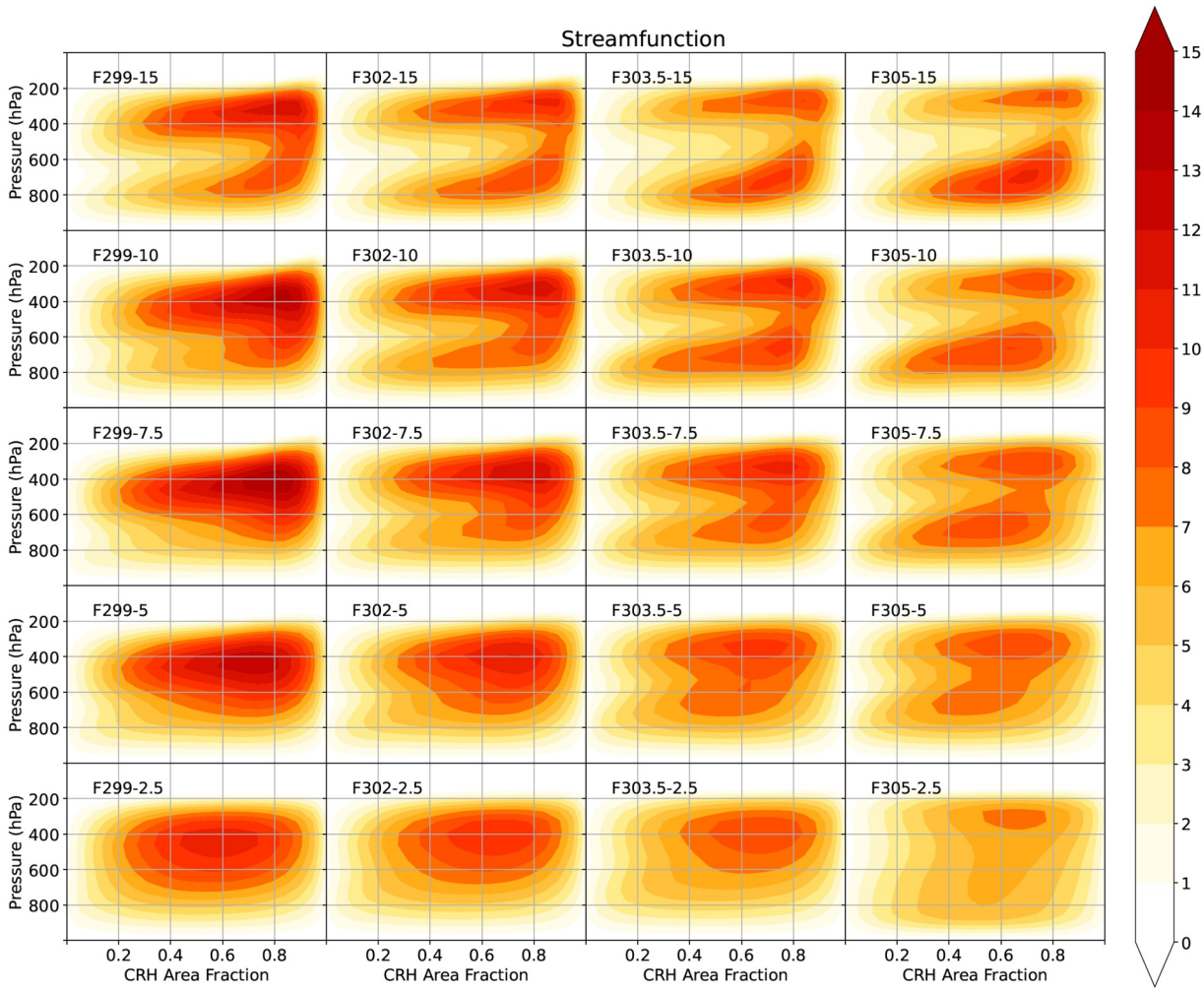


Figure 2. Streamfunction for each case shown in pressure (hPa) and column relative humidity (CRH) area space (%). The global mean SST of each case increases from left to right, and the SST range increases from bottom to top.

increases the upper cell weakens and the shallow cell strengthens and deepens as it expands to higher CRH regions. The weakening of the upper cell is consistent with studies finding that the tropical overturning atmospheric circulation will weaken under warming, primarily because of the increasing dry static stability (Knutson & Manabe, 1995; Vecchi & Soden, 2007). Figure 2 also shows that as the range of SST increases from bottom to top, the shallow circulation strengthens and the circulation takes on a more distinct double cell structure. As the SST range increases, the upper cell tends to shrink toward higher CRH such that the upper cell is strong only over the highest CRH area fractions. So increasing the global mean SST and the SST range both increase the strength of the shallow cell and the double-cell structure of the circulation. It is important to note here that as the SST gradient or mean SST increases and the lower cell strengthens, the circulation also deepens, particularly in the higher CRH value regions of the circulation.

As shown in the bottom row of Figure 2, the circulation in the cases with an SST range of 2.5 K is particularly top heavy and does not have a strong shallow cell. The weak SST gradient is not sufficient to produce strong large-scale organization, given the internal variability of the simulations, and these cases are the least consistent with the others. Even so, the upper cell still rises and weakens with warming, and the circulation starts to show a distinct double cell structure by the warmest experiment, F305–2.5.

Alternative visualizations of the circulation can be found in the Supplemental Material: including an example of the streamfunction in longitude space (Figure S1 in Supporting Information S1) as well as an equivalent figure showing the vertical velocity response of each experiment directly (Figure S2 in Supporting Information S1).

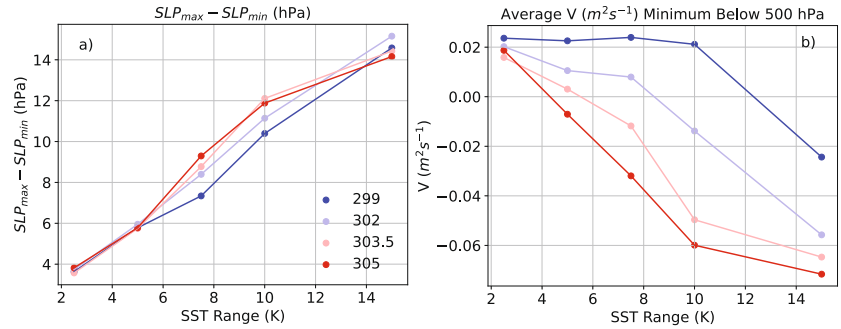


Figure 3. (a) Surface pressure difference from minimum to maximum CRH as a function of SST contrast for each mean temperature. (b) minimum horizontal area velocity (V) averaged over all CRH values for each mean temperature.

Further detail on the response of the circulation to SST is shown in Figure 3. Figure 3a shows that as the SST contrast is increased, the pressure contrast between driest (coldest) and wettest (warmest) portions of the domain increases linearly, with relatively modest sensitivity to mean temperature. This might be expected from the relation of SST to surface pressure predicted by hydrostatic considerations (Lindzen & Nigam, 1987). One would expect these increasing surface pressure gradients to drive a stronger near-surface flow toward warmer SST.

The idealized nature of these experiments allow for a larger-scale than is seen in nature. Wind speeds similarly reach higher values in our idealized experiments than would be expected from typical tropical observations. Zhang et al. (2004) characterize the Shallow Meridional Circulation as having a strong return flow around 600 hPa. This more closely resembles the lower CRH area fraction regions of these experiments. In these experiments, we refer to the strength of this lower cell as the strength of the shallow circulation.

A more direct measure of the relative strength of the shallow circulation is shown in Figure 3b. Here, we show an effective "horizontal area velocity" derived from our expression for streamfunction shown in Equation 2:

$$V = -g\,\frac{d\Psi}{dp} \tag{3}$$

V represents the flow from low to high CRH area fractions, where negative values represent a return flow from high CRH values to low CRH values. Because the shallow circulation is characterized by a strong return flow, we use the strength of this return flow to represent the strength of the shallow circulation. Strong negative values represent a strong return flow and strong shallow circulation. We calculate this index by finding the minimum of V below 500 hPa for each CRH value and taking the average across the full CRH range. This quantity is shown in Figure 3b for each case plotted against SST range. As in Figure 3a, each line represents a different global mean SST. The strength of the return flow increases with both mean SST and SST range. This figure specifically highlights that warming the SST, without increasing the SST gradient, increases the return flow and shallow circulation strength. For the coldest case, the return flow strength only increases at the highest SST range, 15 K. In experiments with already strong shallow circulation strength, such as F303.5-7.5, increasing either the mean SST or SST range appears to have diminishing effects on the return flow associated with the shallow circulation: that is, once a sufficiently large SST mean or range has been reached to create a strong return flow, further increasing the SST mean or range does not strengthen the return flow as much. Increasing either the SST range or warming the mean SST strengthens the shallow circulation, and the strongest shallow circulations occur in experiments with both warm mean SSTs and large SST ranges.

Although we are characterizing these experiments by their mean SST and their SST range, it is important to note that changing either the mean SST or the SST range will also change the maximum SST. The maximum SST is particularly important in the tropics, as the tropospheric air temperature is primarily set by the warmest SSTs (Sobel et al., 2001).

Figure 4 shows the same index for shallow circulation strength used in Figure 3 plotted against the maximum SST for each experiment. The return flow strengthens with maximum SST. The strong and consistent dependence of

21698996, 2026, 20, Downloaded from https://agupubs.onlinelibrary.wiley.com/doi/10.1029/2025JD044828, Wiley Online Library on [23/10/2026]. See the Terms and Conditions (https://onlinelibrary.wiley.com/terms-and-conditions) on Wiley Online Library for rules of use; OA articles are governed by the applicable Creative Commons License

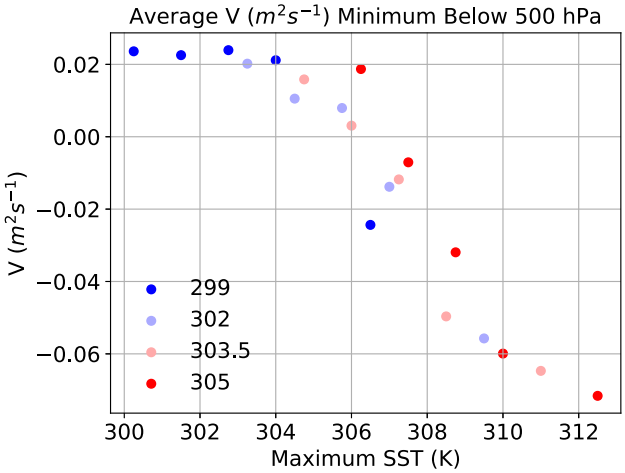


Figure 4. Minimum horizontal area velocity (V) averaged over all CRH values for each mean temperature, plotted against maximum SST. Global mean SST is represented by color.

shallow return flow on the maximum SST suggests that the shallow circulation is related to the vertical profile of temperature and humidity of the atmosphere, which is controlled by the warmest temperatures in the tropics.

3.2. Relative Humidity

The relative humidity is closely tied to both the circulation and the potential mechanisms that drive it. Figure 5 shows contours of relative humidity (%) in pressure versus CRH area fraction. An interesting feature of the relative humidity distribution is a deep secondary moist layer above the near-surface boundary layer. This layer is capped by a sharp transition to much drier air on a surface that slopes downward from the moist to the driest part of the domain. The top of this secondary moist layer depends on the SST mean and range, but, on average, lies around 700 hPa in cold, dry regions and slopes upward to around 500 hPa in the moist, warm regions. This layer becomes thinner and more moist as the SST gradient is increased. Although these models are highly idealized, this middle tropospheric moist layer can be found in observations and reanalysis data. A more detailed description of this secondary moist layer in reanalysis data can be found in Supporting Information S1 (Figure S3 in Supporting Information S1).

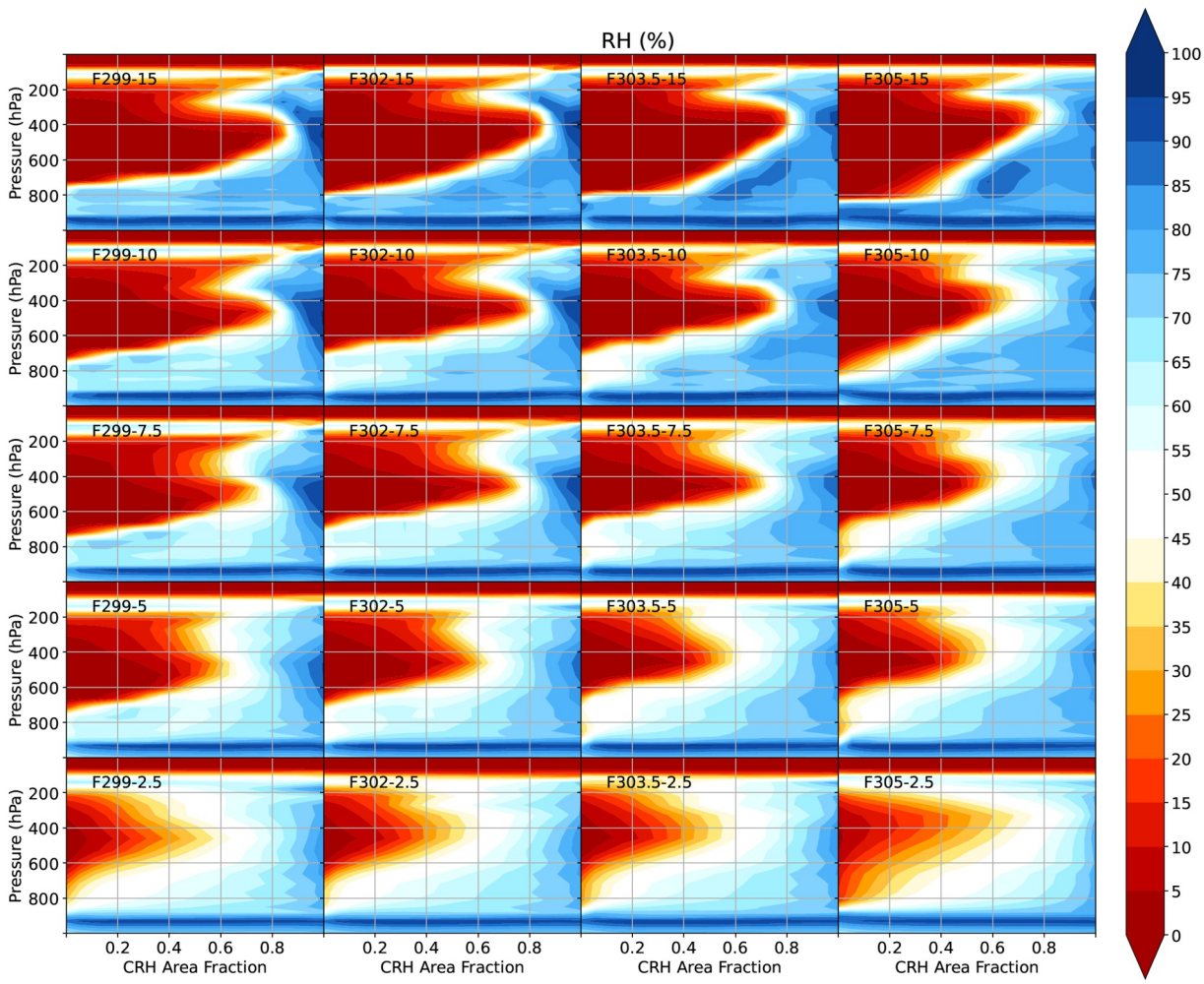


Figure 5. Relative humidity (%) for each case shown in pressure (hPa) and column relative humidity (CRH) area space (%). The global mean SST of each case increases from left to right, and the SST range increases from bottom to top.

21698996, 2026, 20, Downloaded from https://agupubs.onlinelibrary.wiley.com/doi/10.1029/2025JD044828, Wiley Online Library on [23/10/2026]. See the Terms and Conditions (https://onlinelibrary.wiley.com/terms-and-conditions) on Wiley Online Library for rules of use; OA articles are governed by the applicable Creative Commons License

21698996, 2026, 20, Downloaded from https://agupubs.onlinelibrary.wiley.com/doi/10.1029/2025JD044828, Wiley Online Library on [23/10/2026]. See the Terms and Conditions (https://onlinelibrary.wiley.com/terms-and-conditions) on Wiley Online Library for rules of use; OA articles are governed by the applicable Creative Commons License

Later we will show enhanced shallow convection at temperatures just less than the maximum SST in our simulations. This shallow convection deepens and increases in strength with the mean SST, driving stronger shallow circulations in a warmed climate.

Increasing the mean SST and increasing the SST gradient have different effects on the distribution of relative humidity. When increasing the SST range (bottom to top in Figure 5), the subsiding region dries and expands into higher CRH regions. This drying effect is particularly noticeable for the range of CRH area fraction from 0.6 to 0.8. For any given global mean SST, increasing the SST range consistently dries out the mid troposphere (around 600 to 400 hPa) in this CRH window. However, warming the global mean SST while maintaining the same SST contrast has the opposite effect. Warming moistens the layer between 800 and 400 hPa in the window from 0.6 to 0.8 CRH area fraction. We also note here that the changes we are describing are applicable when the double cell structure is present, which requires sufficiently large SST range or gradient for a distinct lower cell to emerge.

The moistening or drying of the 0.6–0.8 CRH window has important effects for radiative cooling and convection. If the air above the boundary layer moistens (dries), longwave cooling of the layer below can be suppressed (enhanced) (Hartmann et al., 2022; Jeevanjee & Fueglistaler, 2020). Conversely, if the air above the boundary layer dries (moistens), convection is suppressed (enhanced). So, the change in relative humidity in this CRH window indicates which mechanism is playing a more active role in strengthening the shallow circulation. When increasing the SST range and drying this CRH window, the conditions are more favorable for longwave cooling. When warming the mean SST and moistening this CRH window, the conditions are more favorable for shallow convection. It is relevant to note here that the relative humidity and these mechanisms feed back on each other, so it is difficult to know which initially triggers the feedback loop. We will discuss in more detail the effect of relative humidity on longwave cooling in Section 4 and on shallow convection in Section 5.

These two mechanisms, increasing the SST gradient and increasing the global mean SST, lead to differing characteristics of the resulting circulation, closely tied to the relative humidity distribution. Increasing the SST gradient leads to a larger dry mid troposphere, with intense convection and precipitation restricted to a smaller area. Increasing the mean SST leads to an increase in shallow convection over intermediate regions, associated with higher mid tropospheric humidity and precipitation over a larger area.

4. Boundary Layer Longwave Cooling

The longwave cooling above the boundary layer in the subsiding region is known to be strongly connected to the shallow circulation strength (Nolan et al., 2007). This relationship is characterized by a feedback between the longwave cooling and the shallow circulation strength through effects on the column relative humidity. As the shallow circulation strengthens, the troposphere of the subsiding region dries and the water vapor above the boundary layer decreases. Decreasing the water vapor path above the emission level leads to an increase in longwave cooling (Hartmann et al., 2022; Jeevanjee & Fueglistaler, 2020). This increase in boundary layer longwave cooling in turn strengthens the shallow circulation (Nolan et al., 2007). Fildier et al. (2023) similarly find the vertical moisture distribution to have a significant role in the long-wave cooling of the boundary layer, and specifically highlight the importance of moist intrusions from remote convection in setting the humidity above the boundary layer.

As shown in Figure 6, for a given global mean SST, as the SST range increases, the magnitude of the longwave cooling also increases. The band of enhanced longwave cooling above the moist layer also expands into the intermediate region between subsidence and deep convection with higher CRH. This enhancement in longwave cooling corresponds to increasing shallow circulation strength and depth, as expected. In summary, we find that the longwave cooling above the boundary layer tends to respond more strongly to an increase in SST range rather than mean SST. This can largely be explained by the relative humidity distribution.

The strength of longwave cooling is directly proportional to the amount of water vapor above the emission level (Fildier et al., 2023; Hartmann et al., 2022; Jeevanjee & Fueglistaler, 2020). Following Hartmann et al. (2022), the cooling-to-space approximation for the longwave cooling rate at a specified emission level and wavelength, λ is a function of its temperature and humidity at that level as well as the vapor pressure path above that level

$$\frac{dT}{dt}|_{\bar{\lambda}} \approx -\left[\frac{\pi g}{C_p e} RHe_s(T) B_{\bar{\lambda}}\right] VPP^{-1} \quad (4)$$

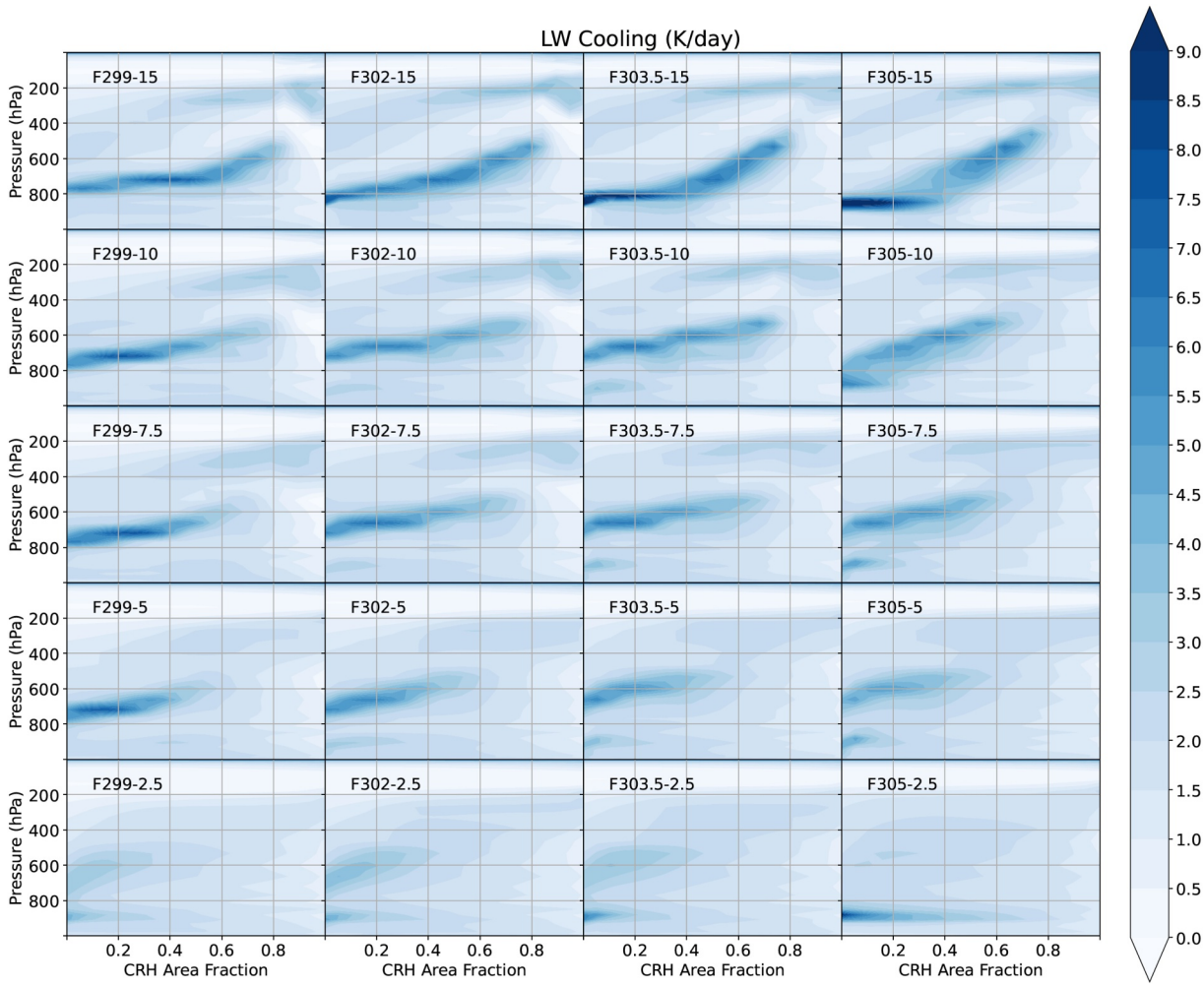


Figure 6. Longwave cooling (K/day) for each case shown in pressure (hPa) and column relative humidity (CRH) area space (%). The global mean SST of each case increases from left to right, and the SST range increases from bottom to top.

where $B_{\tilde{\nu}}(T)$ is the Planck function, $e_s(T)$ is the saturation vapor pressure, C_p is the specific heat at constant pressure, and

$$VPP = \int_0^p RHe_s(T)dp \tag{5}$$

From this expression, we see that the longwave cooling is stronger when the vapor pressure at the emission level is high and the vapor pressure path above the level of emission is small. Figure 7 shows longwave cooling and its relevant components based on the cooling to space approximation shown above by (5). This is broken down further with panels showing the temperature and relative humidity profiles. To show the dependence on SST range, we show the full range of SST gradients for an example mean SST, 303.5 K. We also focus on the intermediate CRH range, 0.6 to 0.8. As described in Section 3.1, the strength of the shallow circulation corresponds to an expansion of the shallow cell to higher CRH area fraction values. Specifically, we identified the CRH area fraction from 0.6 to 0.8 as showing particularly distinct differences between warming and increasing the SST range. So, to analyze the mechanism responsible for this strengthening, we show averages over 0.6–0.8 CRH area fractions. We show experiments with an SST of 303.5 K as a representative example of the changes with increasing SST range.

21698996, 2026, 20, Downloaded from https://agupubs.onlinelibrary.wiley.com/doi/10.1029/2025JD044828, Wiley Online Library on [23/10/2026]. See the Terms and Conditions (https://onlinelibrary.wiley.com/terms-and-conditions) on Wiley Online Library for rules of use; OA articles are governed by the applicable Creative Commons License

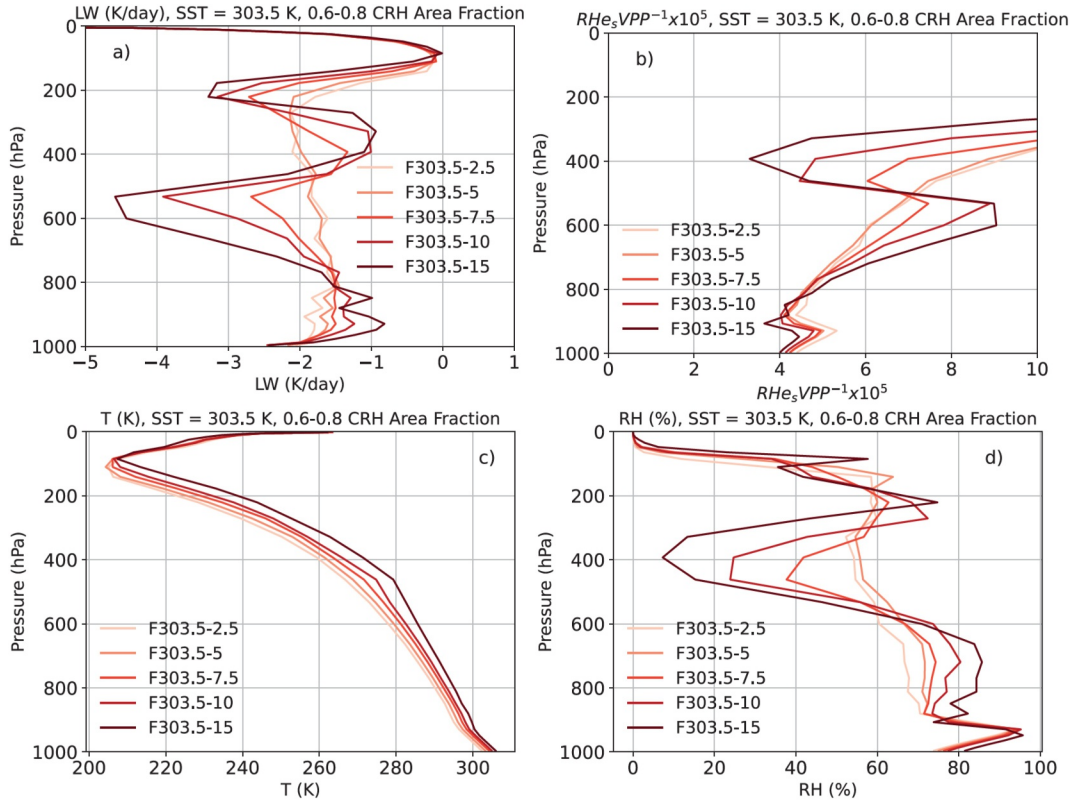


Figure 7. These panels show vertical profiles of quantities corresponding to experiments of each SST range with an SST of 303.5, averaged over 0.6–0.8 CRH area fraction. Panel (a) shows the temperature tendency from longwave cooling (K/day), (b) shows the humidity component of the longwave cooling approximation, $RHe_s(T)VPP^{-1}$, (c) temperature (K), and (d) relative humidity (%).

Figure 7a shows the longwave cooling rates averaged from 0.6 to 0.8 CRH area fraction in pressure coordinates. For this SST and CRH window, the longwave cooling peaks at 532 hPa. Figure 7b shows a peak in $RHe_s(T)VPP^{-1}$ at the same pressure level, indicating strong control of the vapor column on the longwave cooling. The VPP profile peak is a combined effect of both moistening below the emission level and drying above. In addition, because of the large-scale circulation and the weak temperature gradient in the tropics, the temperature of the free troposphere of the entire tropics is set by the warmest region. Figure 7c shows the temperature profiles for each SST range. As the SST range increases, the air temperature increases, and there is a corresponding increase in emission temperature, and thus an increase to the longwave cooling. Because the temperature and consequently the saturation vapor pressure increase with SST range, the reduction in VPP must be dominated by the decrease in relative humidity, shown in Figure 7d.

The VPP above the boundary layer in the subsiding region decreases with increasing SST range. Because the longwave cooling is inversely proportional to the VPP, the longwave cooling is then enhanced with increasing SST gradient. Because the longwave cooling impacts the shallow circulation strength, which in turn impacts the drying above the boundary layer, it is difficult to say whether one causing the other. However, there is a clear trend in the changes in longwave cooling and VPP across changing SST distributions.

In these experiments, increasing the SST range strengthens the large-scale circulation, which dries the mid troposphere in the subsiding region, and increases longwave cooling. So, following the initial drying from the increase in SST range, we see a feedback between the longwave cooling, shallow circulation strength, and humidity of the subsiding region:

1. Drying the subsiding region strengthens the longwave cooling above the boundary layer.
2. Longwave cooling strengthens the shallow circulation.

21698996, 2026, 20, Downloaded from https://agupubs.onlinelibrary.wiley.com/doi/10.1029/2025JD044828, Wiley Online Library on [23/10/2026]. See the Terms and Conditions (https://onlinelibrary.wiley.com/terms-and-conditions) on Wiley Online Library for rules of use; OA articles are governed by the applicable Creative Commons License

3. Moisture transport away from the subsiding region is enhanced, and the vapor pressure above the boundary layer decreases.

Although the feedback described above begins with an increase in SST range strengthening subsidence drying in the free troposphere, because the SST in these experiments is fixed, the circulation changes cannot feedback onto the SST range. In tropical RCE experiments run with interactive SST, the SST distribution oscillates with a speed dependent on the mixed layer depth (Coppin & Bony, 2017, 2018; Dygert & Hartmann, 2023). In this study, we focus instead on the circulation response to an increase in SST range.

5. Shallow Convection

The longwave cooling of the moist layer provides a good consistency argument for the increasing shallow circulation with increasing SST gradient, but this longwave cooling does not work as well in understanding the increase in shallow circulation strength with increasing global mean SST. For a given SST range in Figure 6, as the global mean SST increases, the longwave cooling does not correspond as strongly with the increase in shallow circulation strength with mean SST. We also do not see the same expansion of peak longwave cooling into the intermediate region with increasing mean SST. We know from the streamfunctions shown in Figure 2 that the shallow cell strengthens and expands with increasing global mean SST. Because the longwave cooling does not strengthen and expand (instead, slightly shifting upward) in this region with warming, an alternative explanation for the strengthening of the shallow cell with warming is required.

In this section we explore the role of shallow convection in driving stronger shallow circulations as the mean SST is increased. Figure 8 shows the total heating from parameterized convection in each case. For a given global mean SST, increasing the SST range does increase the strength of both deep and shallow convection, but the convection occupies a narrow region, and does not expand into intermediate regions. When increasing the global mean SST, the shallow convection both intensifies and expands, moistening the mid troposphere over intermediate regions of CRH and SST. In the upper cell, the peak in convective heating is likely associated with latent heat released from the formation of ice clouds (Sokol & Hartmann, 2022). This is therefore dependent on the cloud and precipitation parameterizations, as described in Section 2. We also note here that our shallow convection extends deeper than typically seen in observations. Here, we refer to shallow convection as convection associated with the shallow or lower circulation cell, which in some cases expands into what could be described as "mid-level" convection.

The increase in shallow convection over intermediate SSTs also corresponds to an increase in relative humidity in the layer. To better understand how the increase in shallow convection relates to humidity and sea surface temperature, we use a simplified model. Zhou and Xie (2019) use a spectral plume model (SPM) to illustrate the effect of entrainment on lapse rate. This model computes the effect of entrainment on the temperature of parcels rising in an unsaturated environment. The strength of the entrainment is controlled by a parameter, ϵ, which we set to .3 km^{-1}, which generates temperature profiles that best fit our model data and is also the value chosen by Zhou and Xie (2019) to best fit the observed tropical temperature profile. We use this model to generate parcel profiles for varying relative humidity profiles and sea surface temperatures. We then use these parcel profiles to calculate the convective available potential energy (CAPE), which we expect will explain the location of the shallow convection. Using this simplified model allows us to look at the impact of entrainment drying on convection height, and how this height is influenced by relative humidity.

The total CAPE is defined as

$$\text{CAPE} = \int \frac{T_{v,p} - T_{v,env}}{T_{v,env}} dz \tag{6}$$

where $T_{v,p}$ is the parcel virtual temperature (generated by the SPM) and $T_{v,env}$ is the background virtual temperature (from the GCM data). In model coordinates, this can be written as

$$\text{CAPE} = \sum_i \frac{T_{v,p,i} - T_{v,env,i}}{T_{v,env,i}} \Delta z_i = \sum_i B_i \Delta z_i \tag{7}$$

21698996, 2026, 20, Downloaded from https://agupubs.onlinelibrary.wiley.com/doi/10.1029/2025JD044828, Wiley Online Library on [23/10/2026]. See the Terms and Conditions (https://onlinelibrary.wiley.com/terms-and-conditions) on Wiley Online Library for rules of use; OA articles are governed by the applicable Creative Commons License

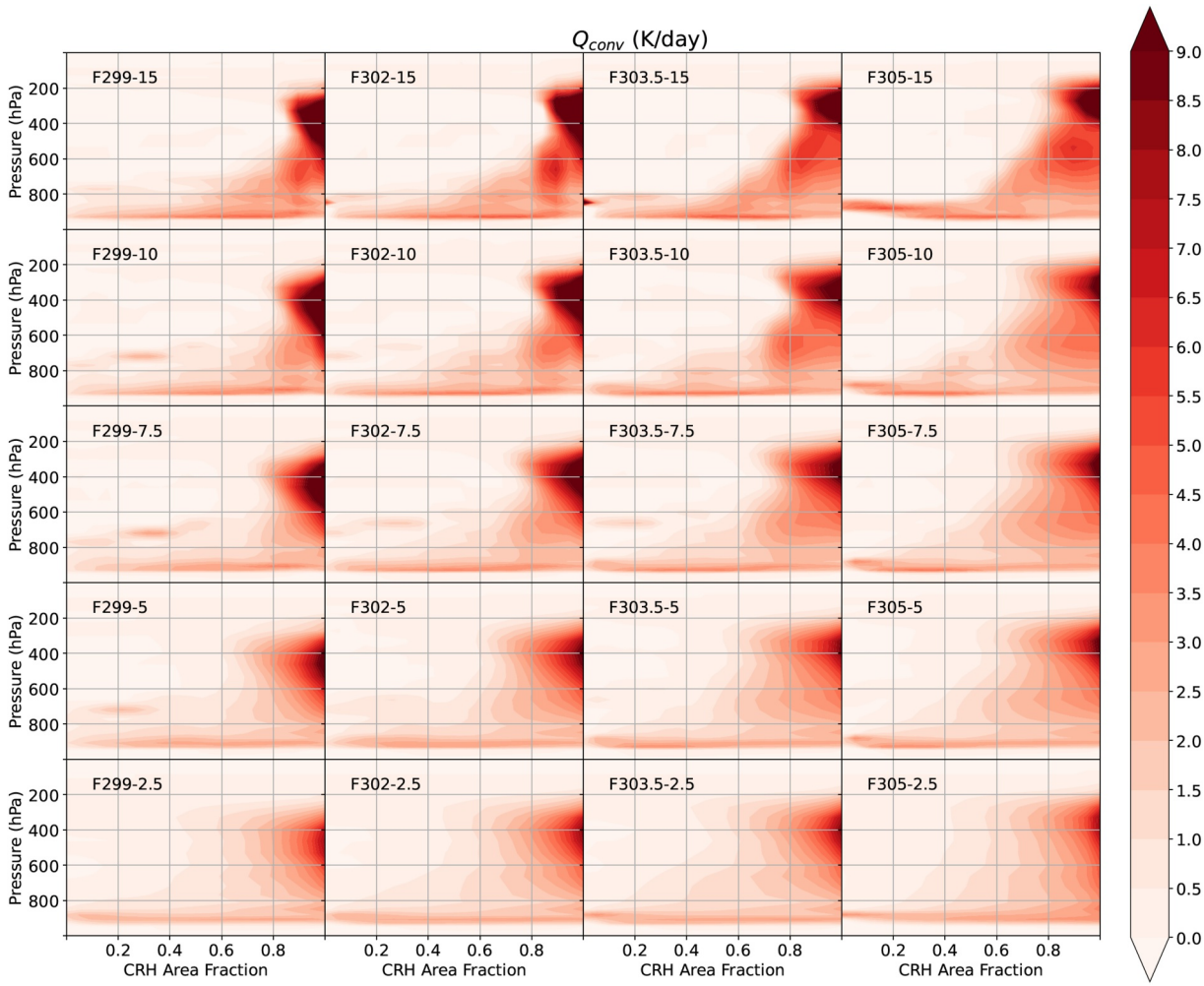


Figure 8. Heating from convection (K/day) for each case shown in pressure (hPa) and column relative humidity (CRH) area space (%). The global mean SST of each case increases from left to right, and the SST range increases from bottom to top.

We call the $B_i \Delta z_i$ at each model level the contribution to CAPE by that layer, and look at how the vertical distribution of this quantity changes from case to case and how this depends on the relative humidity distribution. This quantity is the CAPE generated by the buoyancy from the bottom to the top of each vertical level. This is the buoyancy at the vertical level weighed by the thickness of the slice of that vertical level. So, while we are calculating the CAPE contribution of each vertical level, we are predominantly quantifying the buoyancy.

The top row of Figure 9 shows some test cases to illustrate the role of relative humidity on the vertical profile of CAPE contributions $B_i \Delta z_i$. Shown in green in Figure 9a is the relative humidity in the 0.6–0.8 CRH band for the case F303.5-7.5. In addition, we show test profiles that have a maximum RH of 20%, 40% and 80% above the 849 hPa level. The CAPE contributions calculated with the SPM model for these examples are shown in Figure 9b. Decreasing the relative humidity above 849 hPa relative to the model profile produces a sharp increase of CAPE just above 849 hPa, but this increase is very shallow. This shallow CAPE increase is due to the effect of humidity on virtual temperature. The plume is assumed to be saturated, but the environment is assumed to have the prescribed RH profile. The dry RH profile decreases the virtual temperature of the environment, and so the buoyancy of the saturated parcel increases. This spike in buoyancy is very shallow and above about 750 hPa the CAPE contribution for these dry cases is less than the control case represented by the model. Lifted parcels experience a larger lapse rate when lifted in the drier environment, quickly leading to a colder parcel temperature, and thus reducing the buoyancy of the parcel.

21698996, 2026, 20, Downloaded from https://agupubs.onlinelibrary.wiley.com/doi/10.1029/2025JD044828, Wiley Online Library on [23/10/2026]. See the Terms and Conditions (https://onlinelibrary.wiley.com/terms-and-conditions) on Wiley Online Library for rules of use; OA articles are governed by the applicable Creative Commons License

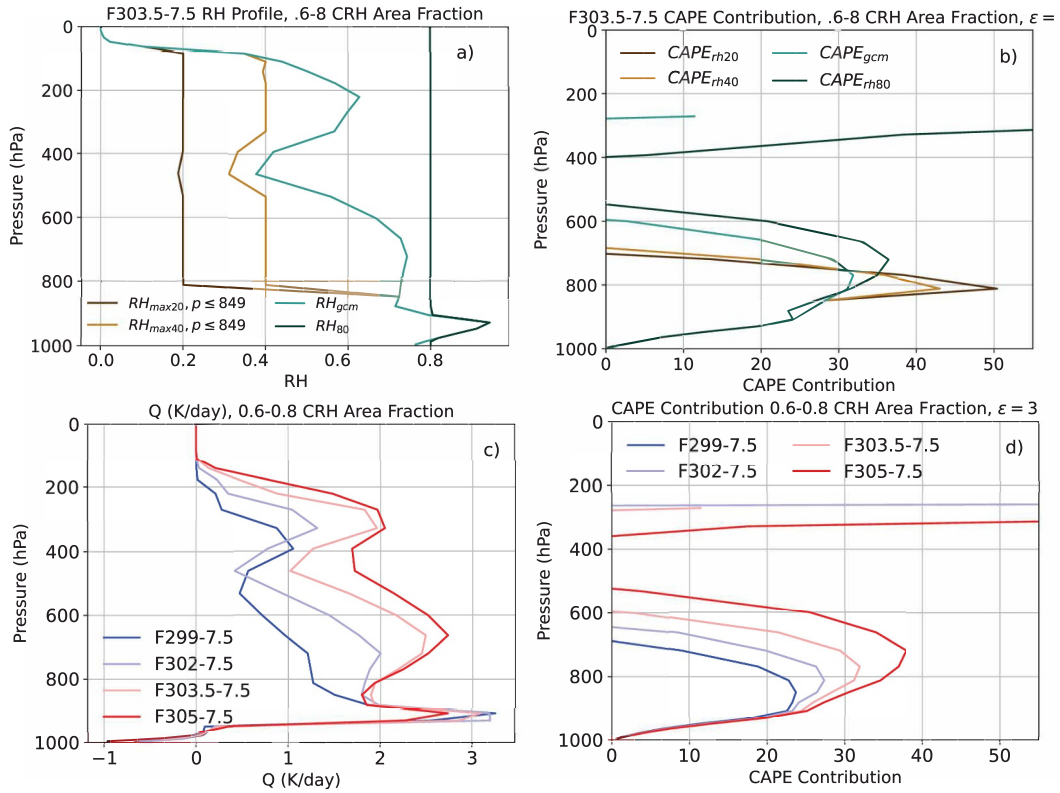


Figure 9. The top row shows the CAPE dependence on relative humidity. Panel (a) shows the relative humidity profiles used to generate parcel profiles in the SPM, (b) the CAPE contribution for each relative humidity profile. The bottom row shows the CAPE dependence on mean SST. Panel c shows the heating from convection (K/day), panel (d) shows the CAPE contribution for cases with a range of 7.5 K.

On the other hand, the SPM predicts a deeper layer of positive CAPE contribution for the moister 80% minimum RH case shown in Figure 9b. Parcels lifted into a moister environment maintain their buoyancy better and lead to increase CAPE contributions.

Figure 9 shows how the CAPE responds to warming in cases with a fixed SST contrast of 7.5 K. Figure 9c shows that the heating from convection in the 800 to 600 hPa layer increases as the temperature is increased from 299 to 305 K, consistent with stronger driving of a shallow circulation by shallow convection as the temperature increases. Figure 9d shows that the plume model CAPE predicts this increase in shallow convection, since the layer of positive CAPE increases and deepens with increasing SST.

Although the magnitude of this effect is sensitive to the entrainment parameter used, the overall effect is consistent: drying limits the height convection reaches, and conversely, moistening can increase the height convection reaches. This is consistent with previous work investigating the impact of environmental humidity on convection (Derbyshire et al., 2004). There is, however, a limit to how much increasing the relative humidity can increase the height of convection. Shown in Figures 9b and 9d, there is a consistent, sharp decline in CAPE contribution around 500 hPa. As the temperature decreases at higher altitudes, the saturation specific humidity decreases, and its effect on the buoyancy and virtual temperature is reduced. Similarly, the effect of drying on the convection height is stronger at lower altitudes where the atmosphere is warmer and specific humidity has a larger impact on the buoyancy.

Janssens et al. (2024) find shallow convection to be the primary driver of mesoscale shallow circulations, and also note that the SST range in the circulations considered is small. Although the mechanisms governing the relationship between convection and circulation may differ between spatial scales (Tomassini, 2020), we find a similar relationship at a much larger scale. Here, we find that shallow convection plays a significant role when warming the global mean SST, and increasing the SST range can actually limit the impact of shallow convection

21698996, 2026, 20, Downloaded from https://agupubs.onlinelibrary.wiley.com/doi/10.1029/2025JD044828, Wiley Online Library on [23/10/2026]. See the Terms and Conditions (https://onlinelibrary.wiley.com/terms-and-conditions) on Wiley Online Library for rules of use; OA articles are governed by the applicable Creative Commons License

21698996, 2026, 20, Downloaded from https://agupubs.onlinelibrary.wiley.com/doi/10.1029/2025JD044828, Wiley Online Library on [23/10/2026]. See the Terms and Conditions (https://onlinelibrary.wiley.com/terms-and-conditions) on Wiley Online Library for rules of use; OA articles are governed by the applicable Creative Commons License

through the drying of the mid troposphere above the moist layer. Dry mid tropospheres strengthen longwave cooling, while moister mid tropospheres favor shallow convection. Shallow convection also brings moisture up from the surface and increases the humidity, making the environment more favorable for future shallow convection.

In these experiments, increasing the global mean SST increases shallow CAPE in the intermediate region between subsidence and deep convection, and this leads to an increase in shallow convection. The moistening and extension of the lower tropospheric moist layer with a warming climate can be clearly seen in the relative humidity sections in Figure 5. A feedback process between shallow convection and relative humidity works as follows:

1. Shallow convection strengthens and enhances the secondary moist layer.
2. A moist lower free troposphere favors shallow convection.

This process becomes stronger with warming as shallow CAPE increases with a warming climate.

6. Summary

Tropical shallow circulations are significant in both observations and in idealized modeling experiments. Potential drivers for shallow circulation strength include boundary layer pressure gradients driven by sea surface temperature distributions, longwave cooling above the boundary layer, and shallow convection. Here, we use an idealized model to look at the relationship between the sea surface temperature gradient, mean sea surface temperature magnitude, and the shallow circulation strength.

We find that different drivers dominate depending on whether we increase the SST range or increase the global mean SST. In both cases, this strengthening of the shallow cell corresponds to anomalous heating rates above the boundary layer. When increasing the SST range, the longwave cooling above the boundary layer in the dry, subsiding region increases as the shallow circulation strengthens. When increasing the global mean SST, the shallow convection over intermediate CRH/SSTs increases, but there is not a strong increase in the longwave cooling above the boundary layer. In summary, increasing the SST range strengthens the shallow circulation by increasing the longwave cooling rate, while increasing the global mean SST strengthens the shallow circulation by increasing the shallow convection over intermediate SSTs.

- When increasing the SST range, the longwave cooling above the boundary layer increases as both the upper-level and shallow circulations strengthen and the subsiding region dries.
- When increasing the global mean SST, heating from shallow convection is the primary mechanism for strengthening the shallow cell. An increase in CAPE over the intermediate region between deep convection and subsidence leads to an increase in shallow convection, moistening the mid troposphere and making the environment more favorable for further convection.
- The conditions favorable for each mechanism work in opposition to each other. Drying above the boundary layer leads to an increase in longwave cooling, but is less favorable for shallow convection due to effects from entrainment drying. Conversely, moistening above the boundary layer is more favorable for shallow convection, but limits the longwave cooling.

These idealized experiments present a simplified, qualitative relationship between these mechanisms and are thus limited in their application to a more realistic setting. For example, the relative humidity in the subsiding region is often much drier than would be expected from observations. This may over-emphasize the significance of entrainment drying on convection. In scenarios with moister subsiding regions, convergence forced shallow convection could play a larger role when increasing the SST gradient, as in Back and Bretherton (2009). Similarly, we use the quantity CAPE in an attempt to connect our results to a quantity applicable to observations, but in our model convection is parameterized. Despite these limitations, these results provide a useful framework for the indirect effect of SST on shallow circulation.

Conflict of Interest

The authors declare no conflicts of interest relevant to this study.

Availability Statement

The model used is Geophysical Fluid Dynamics Laboratory's (GFDL) AM2.1 (Anderson et al., 2004). ERA5 variables are downloaded from the main database (Copernicus Climate Change Service, 2022). Data and code supporting figures can be found on Zenodo (Dygert & Hartmann, 2026).

Acknowledgments
This work was supported by NSF Grant AGS-2124496. We thank the reviewers for their helpful comments and suggestions.

References

Anderson, J., Broccoli, A., Cooke, W., Delworth, T., Dixon, K., Donner, L., et al. (2004). The new GFDL global atmosphere and land model AM2–LM2: Evaluation with prescribed SST simulations. *Journal of Climate*, *17*(24), 4641–4673. https://doi.org/10.1175/jcli-3223.1

Armour, K. C., Proistosescu, C., Dong, Y., Hahn, L. C., Blanchard-Wrigglesworth, E., Pauling, A. G., et al. (2024). Sea-surface temperature pattern effects have slowed global warming and biased warming-based constraints on climate sensitivity. *Proceedings of the National Academy of Sciences*, *121*(12), e2312093121. https://doi.org/10.1073/pnas.2312093121

Back, L. E., & Bretherton, C. S. (2009). On the relationship between SST gradients, boundary layer winds, and convergence over the tropical oceans. *Journal of Climate*, *22*(15), 4182–4196. https://doi.org/10.1175/2009jcli2392.1

Bony, S., Stevens, B., Frierson, D. M. W., Jakob, C., Kageyama, M., Pincus, R., et al. (2015). Clouds, circulation and climate sensitivity. *Nature Geoscience*, *8*(4), 261–268. https://doi.org/10.1038/ngeo2398

Carstens, J. D., & Wing, A. A. (2020). Tropical cyclogenesis from self-aggregated convection in numerical simulations of rotating radiative-convective equilibrium. *Journal of Advances in Modeling Earth Systems*, *12*(5), e2019MS002020. https://doi.org/10.1029/2019ms002020

Copernicus Climate Change Service. (2022). Mass-consistent atmospheric energy and moisture budget monthly data from 1979 to present derived from era5 reanalysis. *ECMWF*. https://doi.org/10.24381/CDS.C2451F6B

Coppin, D., & Bony, S. (2017). Internal variability in a coupled general circulation model in radiative-convective equilibrium. *Geophysical Research Letters*, *44*(10), 5142–5149. https://doi.org/10.1002/2017gl073658

Coppin, D., & Bony, S. (2018). On the interplay between convective aggregation, surface temperature gradients, and climate sensitivity. *Journal of Advances in Modeling Earth Systems*, *10*(12), 3123–3138. https://doi.org/10.1029/2018ms001406

Derbyshire, S. H., Beau, I., Bechtold, P., Grandpeix, J., Piriou, J., Redelsperger, J., & Soares, P. M. M. (2004). Sensitivity of moist convection to environmental humidity. *Quarterly Journal of the Royal Meteorological Society*, *130*(604), 3055–3079. https://doi.org/10.1256/qj.03.130

Dong, Y., Proistosescu, C., Armour, K. C., & Battisti, D. S. (2019). Attributing historical and future evolution of radiative feedbacks to regional warming patterns using a green's function approach: The preeminence of the Western Pacific. *Journal of Climate*, *32*(17), 5471–5491. https://doi.org/10.1175/jcli-d-18-0843.1

Dygert, B. D., & Hartmann, D. L. (2023). The cycle of large-scale aggregation in tropical radiative-convective equilibrium. *Journal of Geophysical Research: Atmospheres*, *128*(7), e2022JD037302. https://doi.org/10.1029/2022jd037302

Dygert, B. D., & Hartmann, D. L. (2026). Effects of sea surface temperature on shallow circulation strength [Dataset]. *model data*. https://doi.org/10.5281/zenodo.22845609

Fildier, B., Muller, C., Pincus, R., & Fueglistaler, S. (2023). How moisture shapes low-level radiative cooling in subsidence regimes. *AGU Advances*, *4*(3), e2023AV000880. https://doi.org/10.1029/2023av000880

Fläschner, D., Mauritsen, T., Stevens, B., & Bony, S. (2018). The signature of shallow circulations, not cloud radiative effects, in the spatial distribution of tropical precipitation. *Journal of Climate*, *31*(23), 9489–9505. https://doi.org/10.1175/jcli-d-18-0230.1

Grabowski, W. W., Yano, J.-I., & Moncrieff, M. W. (2000). Cloud resolving modeling of tropical circulations driven by large-scale SST gradients. *Journal of the Atmospheric Sciences*, *57*(13), 2022–2040. https://doi.org/10.1175/1520-0469(2000)057⟨2022:crmotc⟩2.0.co;2

Hartmann, D. L., & Dygert, B. D. (2022). Global radiative convective equilibrium with a slab ocean: SST contrast, sensitivity and circulation. *Journal of Geophysical Research: Atmospheres*, *127*(12), e2021JD036400. https://doi.org/10.1029/2021jd036400

Hartmann, D. L., Dygert, B. D., Blossey, P. N., Fu, Q., & Sokol, A. B. (2022). The vertical profile of radiative cooling and lapse rate in a warming climate. *Journal of Climate*, *35*(19), 6253–6265. https://doi.org/10.1175/jcli-d-21-0861.1

Huaman, L., Schumacher, C., & Sobel, A. H. (2022). Assessing the vertical velocity of the east Pacific itcz. *Geophysical Research Letters*, *49*(1), e2021GL096192. https://doi.org/10.1029/2021gl096192

Jakob, C., & Klein, S. A. (2000). A parametrization of the effects of cloud and precipitation overlap for use in general-circulation models. *Quarterly Journal of the Royal Meteorological Society*, *126*(568), 2525–2544. https://doi.org/10.1256/smsqj.56808

Janssens, M., George, G., Schulz, H., Couvreux, F., & Bouniol, D. (2024). Shallow convective heating in weak temperature gradient balance explains mesoscale vertical motions in the trades. *Journal of Geophysical Research: Atmospheres*, *129*(18), e2024JD041417. https://doi.org/10.1029/2024jd041417

Jeevanjee, N., & Fueglistaler, S. (2020). On the cooling-to-space approximation. *Journal of the Atmospheric Sciences*, *77*(2), 465–478. https://doi.org/10.1175/jas-d-18-0352.1

Knutson, T. R., & Manabe, S. (1995). Time-mean response over the tropical Pacific to increased c02in a coupled ocean-atmosphere model. *Journal of Climate*, *8*(9), 2181–2199. https://doi.org/10.1175/1520-0442(1995)008⟨2181:tmrott⟩2.0.co;2

Larson, K., & Hartmann, D. L. (2003). Interactions among cloud, water vapor, radiation, and large-scale circulation in the tropical climate. Part ii: Sensitivity to spatial gradients of sea surface temperature. *Journal of Climate*, *16*(10), 1441–1455. https://doi.org/10.1175/1520-0442(2003)016⟨1441:IACWVR⟩2.0.CO;2

Lindzen, R. S., & Nigam, S. (1987). On the role of sea surface temperature gradients in forcing low-level winds and convergence in the tropics. *Journal of the Atmospheric Sciences*, *44*(17), 2418–2436. https://doi.org/10.1175/1520-0469(1987)044⟨2418:otross⟩2.0.co;2

Lutsko, N. J., & Cronin, T. W. (2018). Increase in precipitation efficiency with surface warming in radiative-convective equilibrium. *Journal of Advances in Modeling Earth Systems*, *10*(11), 2992–3010. https://doi.org/10.1029/2018ms001482

Lutsko, N. J., & Cronin, T. W. (2024). The transition to double-celled circulations in mock-Walker simulations. *Geophysical Research Letters*, *51*(14), e2024GL108945. https://doi.org/10.1029/2024gl108945

Moorthi, S., & Suarez, M. J. (1992). Relaxed Arakawa-Schubert. A parameterization of moist convection for general circulation models. *Monthly Weather Review*, *120*(6), 978–1002. https://doi.org/10.1175/1520-0493(1992)120⟨0978:rasapo⟩2.0.co;2

Naumann, A. K., Stevens, B., Hohenegger, C., & Mellado, J. P. (2017). A conceptual model of a shallow circulation induced by prescribed low-level radiative cooling. *Journal of the Atmospheric Sciences*, *74*(10), 3129–3144. https://doi.org/10.1175/jas-d-17-0030.1

Nishant, N., Sherwood, S. C., & Geoffroy, O. (2016). Radiative driving of shallow return flows from the itcz. *Journal of Advances in Modeling Earth Systems*, *8*(2), 831–842. https://doi.org/10.1002/2015ms000606

21698996, 2026, 20, Downloaded from https://agupubs.onlinelibrary.wiley.com/doi/10.1029/2025JD044828, Wiley Online Library on [23/10/2026]. See the Terms and Conditions (https://onlinelibrary.wiley.com/terms-and-conditions) on Wiley Online Library for rules of use; OA articles are governed by the applicable Creative Commons License

Nolan, D. S., Zhang, C., & Chen, S.-h. (2007). Dynamics of the shallow meridional circulation around intertropical convergence zones. *Journal of the Atmospheric Sciences*, *64*(7), 2262–2285. https://doi.org/10.1175/jas3964.1

Rotstayn, L. D. (1997). A physically based scheme for the treatment of stratiform clouds and precipitation in large-scale models. I: Description and evaluation of the microphysical processes. *Quarterly Journal of the Royal Meteorological Society*, *123*(541), 1227–1282. https://doi.org/10.1256/smsqj.54105

Rotstayn, L. D., Ryan, B. F., & Katzfey, J. J. (2000). A scheme for calculation of the liquid fraction in mixed-phase stratiform clouds in large-scale models. *Monthly Weather Review*, *128*(4), 1070–1088. https://doi.org/10.1175/1520-0493(2000)128<1070:asfcot>2.0.co;2

Schulz, H., & Stevens, B. (2018). Observing the tropical atmosphere in moisture space. *Journal of the Atmospheric Sciences*, *75*(10), 3313–3330. https://doi.org/10.1175/jas-d-17-0375.1

Sobel, A. H., & Neelin, J. D. (2006). The boundary layer contribution to intertropical convergence zones in the quasi-equilibrium tropical circulation model framework. *Theoretical and Computational Fluid Dynamics*, *20*(5–6), 323–350. https://doi.org/10.1007/s00162-006-0033-y

Sobel, A. H., Nilsson, J., & Polvani, L. M. (2001). The weak temperature gradient approximation and balanced tropical moisture waves. *Journal of the Atmospheric Sciences*, *58*(23), 3650–3665. https://doi.org/10.1175/1520-0469(2001)058⟨3650:twtgaa⟩2.0.co;2

Sokol, A. B., & Hartmann, D. L. (2022). Radiative cooling, latent heating, and cloud ice in the tropical upper troposphere. *Journal of Climate*, *35*(5), 1643–1654. https://doi.org/10.1175/jcli-d-21-0444.1

Tiedtke, M. (1993). Representation of clouds in large-scale models. *Monthly Weather Review*, *121*(11), 3040–3061. https://doi.org/10.1175/1520-0493(1993)121<3040:rocils>2.0.co;2

Tokioka, T., Yamazaki, K., Kitoh, A., & Ose, T. (1988). The equatorial 30-60 day oscillation and the Arakawa-Schubert penetrative cumulus parameterization. *Journal of the Meteorological Society of Japan. Series II*, *66*(6), 883–901. https://doi.org/10.2151/jmsj1965.66.6_883

Tomassini, L. (2020). The interaction between moist convection and the atmospheric circulation in the tropics. *Bulletin of the American Meteorological Society*, *101*(8), E1378–E1396. https://doi.org/10.1175/bams-d-19-0180.1

Vecchi, G. A., & Soden, B. J. (2007). Global warming and the weakening of the tropical circulation. *Journal of Climate*, *20*(17), 4316–4340. https://doi.org/10.1175/jcli4258.1

Yano, J.-I., Grabowski, W. W., & Moncrieff, M. W. (2002). Mean-state convective circulations over large-scale tropical SST gradients. *Journal of the Atmospheric Sciences*, *59*(9), 1578–1592. https://doi.org/10.1175/1520-0469(2002)059⟨1578:msccol⟩2.0.co;2

Zhang, C., McGauley, M., & Bond, N. A. (2004). Shallow meridional circulation in the tropical Eastern Pacific. *Journal of Climate*, *17*(1), 133–139. https://doi.org/10.1175/1520-0442(2004)017⟨0133:smcitt⟩2.0.co;2

Zhang, C., Nolan, D. S., Thorncroft, C. D., & Nguyen, H. (2008). Shallow meridional circulations in the tropical atmosphere. *Journal of Climate*, *21*(14), 3453–3470. https://doi.org/10.1175/2007jcli1870.1

Zhou, W., & Xie, S.-P. (2019). A conceptual spectral plume model for understanding tropical temperature profile and convective updraft velocities. *Journal of the Atmospheric Sciences*, *76*(9), 2801–2814. https://doi.org/10.1175/jas-d-18-0330.1

References From the Supporting Information

Hersbach, H., Bell, B., Berrisford, P., Hirahara, S., Horányi, A., Muñoz-Sabater, J., et al. (2020). The era5 global reanalysis. *Quarterly Journal of the Royal Meteorological Society*, *146*(730), 1999–2049. https://doi.org/10.1002/qj.3803

21698996, 2026, 20, Downloaded from https://agupubs.onlinelibrary.wiley.com/doi/10.1029/2025JD044828, Wiley Online Library on [23/10/2026]. See the Terms and Conditions (https://onlinelibrary.wiley.com/terms-and-conditions) on Wiley Online Library for rules of use; OA articles are governed by the applicable Creative Commons License